Experimental Neurology 320 (2019) 112980

Contents lists available at ScienceDirect

Experimental Neurology

journal homepage: www.elsevier.com/locate/yexnr

Research paper

Physical impacts of PLGA scaffolding on hMSCs: Recovery neurobiology insight for implant design to treat spinal cord injury

In-Bo Han[a,b,1,2], Devang K. Thakor[a,b,1], Alexander E. Ropper[a,b,1], Dou Yu[a,b], Lei Wang[a,b], Serdar Kabatas[a,b], Xiang Zeng[a,b], Soo-Woo Kim[c], Ross D. Zafonte[a], Yang D. Teng[a,b,*]

[a] Departments of Physical Medicine & Rehabilitation and Neurosurgery, Harvard Medical School/Spaulding Rehabilitation Hospital/Brigham and Women's Hospital, Boston, MA, USA
[b] Division of SCI Research, Veterans Affairs Boston Healthcare System, Boston, MA, USA
[c] Division of Periodontology, Harvard School of Dental Medicine, Boston, MA, USA

ARTICLE INFO

Keywords:
Functional multipotency of stem cells
Mechanotransduction
Mesenchymal stromal stem cell
Poly(d,l-lactic-*co*-glycolic acid)
Polymeric scaffold
Recovery neurobiology
Rigidity
Spinal cord injury

ABSTRACT

Our earlier work generated a powerful platform technology of polymeric scaffolding of stem cells to investigate and treat the injured or diseased central nervous system. However, the reciprocal sequelae between biophysical properties of the polymer and responses of the stem cell have not been examined in situ in lesioned spinal cords. We postulated that implantable synthetic scaffolds, acting through physical features, might affect donor cell behavior and host tissue remodeling. To test this hypothesis, poly(d,l-lactic-*co*-glycolic acid) (PLGA) in either low/soft or high/hard rigidity was fabricated for carrying adult human bone marrow mesenchymal stromal stem cells (hMSCs). The construct was transplanted into the epicenter of a rat model of acute T9–10 segmental hemisection to evaluate the effect of PLGA rigidity on the therapeutic potential and fate of hMSCs for neural repair. Compared to controls, only treatment with soft PLGA-scaffolded hMSCs significantly improved sensorimotor function via activation of recovery neurobiology mechanisms. The main benefits included inhibiting neuroinflammation and enhancing tissue protection. Also detected in the treated lesion region were expressions of neurotrophic and anti-inflammatory factors together with proliferation of endogenous neural stem cells, impacts likely derived from hMSCs' functional multipotency maintained by soft PLGA-scaffolding. Conversely, hard rigidity PLGA activated mechanotransduction and mesoderm lineage differentiation of hMSCs that ectopically produced bone, cartilage and muscle markers in neural parenchyma. The findings collectively suggested that the physical texture of polymeric scaffolds should be tailored for sustaining the stemness of hMSCs to constructively interact with the spinal cord for functional restoration.

1. Introduction

Reports of functional recovery from spinal cord injury (SCI) after transplantation of human mesenchymal stromal stem cells (hMSCs) have generated high expectations for developing and installing clinical cell therapies for neurotrauma (Spejo et al., 2018; Papa et al., 2018; Ropper et al., 2017; Bao et al., 2011; Hofstetter et al., 2002; Cyranoski, 2019). However, certain experimental and clinical studies only showed very limited benefits following intraparenchymal administration of hMSCs, due to poor donor survival in a hostile microenvironment of the injured adult mammalian spinal cord (Oh et al., 2016; Ohta et al., 2004). Using a unique in vitro organotypic coculture system, we recently demonstrated that soft texture PLGA provided support to functional multipotency of hMSCs to exert neural repair effects on adult rat dorsal root ganglia (DRG) explants (Thakor et al., 2018) and lesioned spinal cords via maintaining hMSCs' stemness capacity (Ropper et al., 2017; Teng, 2019a).

The studies were enabled by a platform technology our collaborators and we originally devised, which established 3-dimensional (3D) biodegradable polymer-based neural stem cell (NSC) transplantation systems mimicking spinal cords for research and therapeutic development (Teng et al., 2002; Park et al., 2002). We later further enhanced the design of the polymeric construct by adding controlled drug release and stemness retention features (Yu et al., 2009; Thakor et al., 2018)

* Corresponding author at: Departments of PM&R and Neurosurgery, Harvard Medical School, Spaulding Rehabilitation Hospital, Brigham & Women's Hospital, and Veterans Affairs Boston Healthcare System, Boston, MA, USA.
E-mail address: yang_teng@hms.harvard.edu (Y.D. Teng).
[1] I.B.H., D.K.T. and A.E.R. contributed equally to this study.
[2] Present address: Department of Neurosurgery, CHA University, School of Medicine, Bundang CHA Medical Center, Sungnam, Korea (I.B.H.)

https://doi.org/10.1016/j.expneurol.2019.112980
Received 18 April 2019; Received in revised form 5 June 2019
Available online 20 June 2019

and uncovered Functional Multipotency of Stem Cells (Teng et al., 2008, 2010, 2011; Teng, 2019a & b). The elevated functional repair efficacies of polymer-scaffolded NSCs were corroborated by independent findings from other laboratories (Kubinova et al., 2011; Cigognini et al., 2011; Hwang et al., 2011). Overall, the outcomes suggested that synthetic scaffolds should physically and biochemically emulate the microenvironment of the host tissue and/or donor cell developmental niche to optimize therapeutic potential.

MSCs have been known for their sensitivity to mechanically transduced cues from the surroundings. They can differentiate into various mesoderm lineages depending on the rigidity of the extracellular matrix molecules (ECM) that underlie the stiffness of the structure (Hejcl et al., 2010; Dupont et al., 2011; Engler et al., 2006). Functional multipotency of MSCs is maintained by stemness biology (Thakor et al., 2018), which permits the cells, in interactive manner, to secrete trophic factors and cytokines, and to form gap junctions besides phenotypic differentiation (Teng, 2019a). We thereby reasoned that the mechanical properties of PLGA scaffolds might influence stemness-based therapeutic capacity of hMSCs and host tissue response. The hypothesis was tested in an adult rat model of T9–10 segmental hemisection.

2. Materials and methods

2.1. Fabrication of PLGA scaffolds

The scaffolds were prepared as previously described by our group (Teng et al., 2002; Ropper et al., 2017; Thakor et al., 2018). In particular, the scaffolds were synthesized from a blend of 75% PLGA:25% PLGA-polylysine (PLGA-PLL) (*w/w*) (PLGA: 50:50 lactide:glycolide, Mn 30,000 to 60,000 Da, Sigma-Aldrich cat no. P2191; PLGA-PLL: PLGA block Mn ~30,000 Da, polylysine block Mn ~10,000 Da, PolySciTech, cat. No. AI028). Hereafter, this blend is referred to as "PLGA" for simplicity. The PLGA blend was dissolved in chloroform and cast over salt with a particle diameter range of 350–500 μm (made from rock salt; Thermo Fisher Scientific cat. no. S71989) inside a glass vial to a volume ratio of ~2:1 (salt:PLGA solution). The chloroform solvent was then allowed to evaporate under an organic solvent-resistant desiccator. After drying, the salt/PLGA construct was cut from the glass vial and soaked overnight in sterilized distilled water to leach out the salt, followed by a series of washes with fresh sterile distilled water (Fig. 1A_{1-4}). This salt-leaching process produced pores in sizes of 350–500 μm. The porous scaffolds were then allowed to dry in a laminar flow hood and cut to the implant size (W × H × L: 1 × 2 × 4 mm). The scaffolds were stored at −20 °C until use.

To obtain PLGA scaffolds of different stiffness, the elasticity was manipulated by varying the concentration of PLGA (i.e., 10, 20, and 40%) in the solvent during scaffold casting in the molds (Fig. 1B_1), or by treating the scaffolds with ultraviolet (UV) for different times (Fig. 1B_2) or NaOH at different concentrations (Fig. 1B_3). In our experience a higher concentration of PLGA could produce a denser, more rigid scaffold than a lower PLGA concentration. Thus, a standard PLGA concentration of 20% was compared to 40% and 10% for fabricating stiffer and softer scaffolds, respectively. Furthermore, based on a previous report (Yixiang et al., 2008), we exposed the scaffold made of 40% PLGA to UV irradiation to soften it via partial PLGA degradation, resulting in reduced tensile strength of polymer nanofibers. These scaffolds were compressed after incubation in cell culture medium for 4 days. Lastly, because NaOH treatment could degrade PLGA through hydrolysis of ester bonds by hydroxide anions (Vance et al., 2004; Colzani et al., 2018) we used 0.1 or 1.0 M NaOH treatment to soften the 40% PLGA scaffolds.

For stiffness evaluation, the scaffolds were compressed using a 75 g aneurysm clip (Mizuho America Inc., Union City, CA), and the ratio of the final to the initial width along the axis of compression (red arrows in Fig. 1B_4) was used to define the compressibility as an outcome measure of physical stiffness.

2.2. Cell culture

hMSCs were obtained from either a 26 year-old male donor (7023R) or a 29 year-old female donor (7038-L) at the Tulane University Center for Gene Therapy, an NIH funded cell repository center (Ropper et al., 2017; Thakor et al., 2018). hMSCs were maintained in Dulbecco's modified eagle medium (DMEM) (GibcoBRL, Grand Island, NY) containing 15% fetal bovine serum (Invitrogen) and 1% penicillin-streptomycin (Invitrogen). The medium was changed every three days. The cells were stored in a cell culture incubator at 37 °C under a 5% CO_2 atmosphere and were passaged every 6–7 days when they were at 80–90% confluency.

To control for quality of stemness, a fraction of hMSCs in each culture passage was used for immunocytochemical (ICC) analysis to determine the expression profile of MSC-specific markers. For study inclusion, passages must have ≥90% of the cells expressing hMSC markers (e.g., HLA−I, CD147, CD90, CD105, CD49c, and/or CD29) without presentation of non-hMSC markers (e.g., CD36, CD34, CD19, and CD11b). In general, hMSCs with less than six cell passages (< 6P) met the aforementioned criteria and were used for scaffold seeding.

2.3. Preparation of PLGA scaffold and feeder hMSC monolayer

Scaffolds were soaked in 70% ethanol at room temperature for at least 3 h to permit disinfection and hydration. The scaffolds were washed (10 min × 3) under sterile conditions in phosphate-buffered saline (1× PBS: 10 mM $PO4^{3-}$, 137 mM NaCl, and 2.7 mM KCl; pH: ~7.4 and osmolality: 280–315 mOsm/kg; Sigma-Aldrich). The scaffolds were incubated in 100% FBS containing 1% penicillin-streptomycin (both from Thermo Fisher Scientific) overnight to permit the adsorption of serum proteins to facilitate hMSCs attachment. To increase the seeding of hMSCs onto the soft scaffolds, feeder hMSCs (at the 16th passage) were plated onto the bottom of Corning® Costar® TC-Treated 24-well plates (Sigma-Aldrich) at a density of 1×10^4 cells/cm^2, and the soft scaffolds were placed onto these feeder cells the next day. The hard scaffolds were placed into the 24-well plate for direct donor cell engrafting, since there were ~3× more hMSCs per hard scaffold than a soft scaffold after the same process of adding cells without exposure to any feeder cells (see below). To probe the influence of PLGA rigidity over therapeutic potential and fate of hMSCs in lesioned spinal cords, we decided to use an identical procedure for cell seeding per se for the two groups without implementing the same feeder treatment or number of hMSCs per scaffold.

2.4. Seeding and culture of hMSCs in PLGA scaffolds

For cell seeding onto the soft scaffolds, 5 μl of a suspension of low-passage (< P6) hMSCs (2×10^4 cells/μl) was pipetted slowly into the medium over the polymer surface. The scaffolds were maintained in a 37 °C/5% CO_2 incubator (Model: CO-150; New Brunswick Scientific, Edison, NJ) for 3 h to permit cell attachment prior to addition of 1 ml fresh medium to each well. The seeding procedure was repeated at 24 and 48 h after the initial seeding. In total, ~6×10^4 cells were seeded in each soft scaffold based on the estimate derived from cell quantification of 20 μm sections of the implant following H&E staining. For seeding onto the hard scaffolds, 6 μl of a low-passage (< P6) hMSC suspension (6×10^4/μl) was pipetted over the top of a polymer construct, followed with 37 °C/5% CO_2 incubation for 3 h and medium replenishment. After the same formula of repeated seeding, ~1.8×10^5 cells were seeded in each hard scaffold (i.e., ~3× more cells in each hard scaffold than onto a soft scaffold). All scaffold-cell implants were then returned to the incubator and continuously cultured for 3 days prior to transplantation.

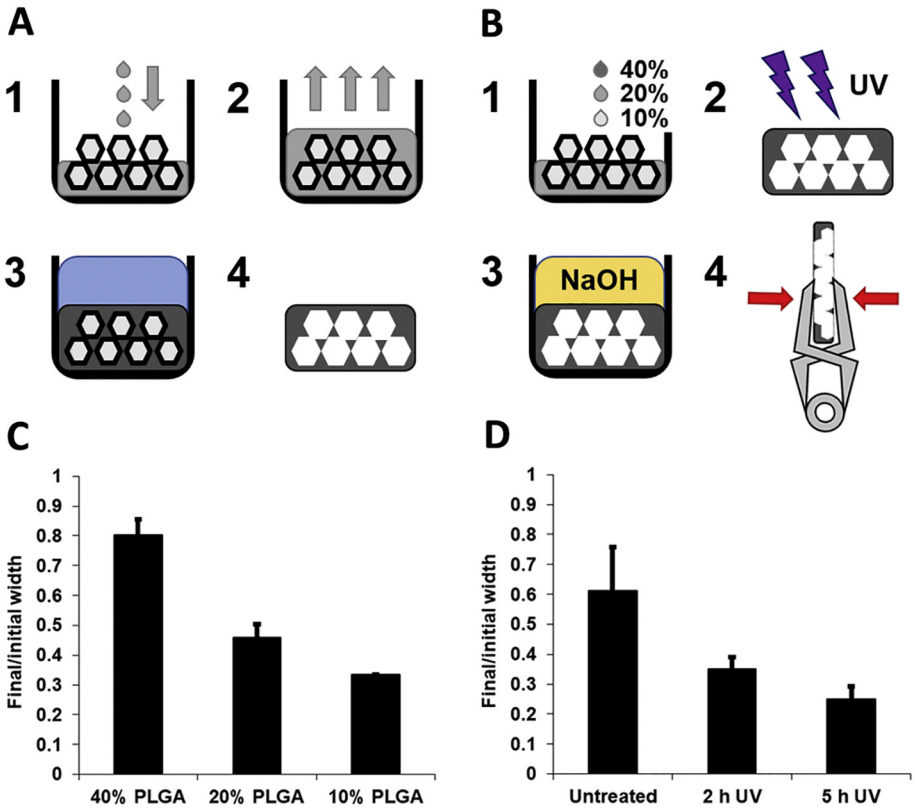

Fig. 1. Establishment of PLGA scaffolds in varying rigidity and stiffness.
A. Scaffold synthesis. 1: Casting of PLGA blend dissolved in chloroform over salt particles. 2: Evaporation of chloroform solvent, leaving solid scaffold. 3: Soaking of scaffold in water to dissolve salt particles, generating pores. 4: Finished product of porous scaffolds. B. Methods for manipulating and testing stiffness. 1: Different concentrations of the PLGA blend in the solvent. 2: Ultraviolet (UV) irradiation. 3: NaOH treatment. 4: Stiffness testing. Compressibility was used to define stiffness as a function of rigidity. It was determined by comparing the initial and final widths (measured alongside the red arrows) of the scaffolds after 1 min compression of a 75 g force applied from an aneurysm clip. C. Compressibility of scaffolds prepared with different concentrations of PLGA. Scaffolds were compressed when dry. D. Compressibility of scaffolds prepared from 40% PLGA and subjected to UV irradiation for different times. Scaffolds were compressed immediately after incubation in cell culture medium for 4 days. (For interpretation of the references to colour in this figure legend, the reader is referred to the web version of this article.)

2.5. Implantation of the hMSC-seeded scaffolds

After approval by the Institutional Animal Care and Use Committee of Harvard Medical School and in accordance with its guidelines, female Sprague-Dawley rats weighing 220–250 g (Charles River Labs, Wilmington, MA) underwent unilateral midline hemisection at the T9-T10 level as previously described (Teng et al., 2002; Yu et al., 2009; Ropper et al., 2017). Surgeries and implantations were performed in a randomized block design. Briefly, rats were anesthetized with intraperitoneal injections of ketamine/xylazine mixture (70–100 mg/kg and 10–20 mg/kg; Sigma-Aldrich) and a laminectomy was performed from the ninth to the tenth thoracic vertebrae, followed by a left lateral midline hemisection at the T_9-T_{10} spinal cord to generate a 4-mm longitudinal gap using a size 11 Bard-Parker® disposable sharp scalpel (Aspen Surgical, Caledonia, MI). Following parenchyma removal via negative pressure suction, the surgical blade was repeatedly scraped along the ventral surface of the spinal canal to sever any residual fibers at the lesion epicenter before one of the following treatments was given (Teng et al., 2002; Yu et al., 2009; Ropper et al., 2017). In total, 4 treatment or control designs were studied (n = 7/group): (1) lesion alone control group; (2) hard PLGA scaffold alone (without hMSCs) group; (3) hard PLGA-scaffolded hMSC group; and (4) soft PLGA-scaffolded hMSC group. The soft scaffold without cell seeding showed high degree of shrinkage upon hydration, which tripled the polymer amount that was required to fill the epicenter lesion gap, disqualifying its use as an adequate vehicle material in this SCI model. In addition, our published reports demonstrated that without proper scaffolding hMSCs or hNSCs would quickly die in the lesion gap of this SCI model (Teng et al., 2002; Yu et al., 2009; Ropper et al., 2017). For these reasons no control groups were set up to receive soft scaffold alone and hMSC suspension only. After each procedure, hemostasis was achieved via using Gelfoam® (Pfizer, New York, NY); the muscles and skin were closed with sutures and wound clips (Leica Biosystems), respectively. All post-surgery animals received buprenorphine administration (0.01–0.05 mg/kg/day, s.c.) for 5 consecutive days to manage potential nociceptive sensory responses. The bladders were expressed manually twice per day until a so called reflex bladder was established (Teng et al., 2002; Ropper et al., 2017).

2.6. Behavioral analysis

On the first day after SCI and then once weekly thereafter throughout the entire study, standard behavioral evaluations were performed by two observers blinded to the treatment (Teng et al., 2002, 2004). At each time point, a battery of tests was used to examine the coordinated use and reflexes of the hindlimbs. For coordinated motor function, the Basso-Beattie-Bresnahan (BBB) scale of ranking open field locomotor ability was assessed, which ran from 0 (total paralysis) to 21 (normal). In addition, the downward-facing inclined plane performance was evaluated to measure the maximum degree of plane inclination where a rat could maintain a stable body position for 5 s. Spinal cord reflex tests monitored hindlimb toe spreading, placing, and withdrawal response to extension, pressure, or brief pain stimulation, as well as contact righting reflex. For these examinations, the scores range was 0 (no response to the stimulus), 1 (reduced response), 2 (normal response), and 3 (hyperactive response). The withdrawal response to Semmes-Weinstein filament stimulation was also tested. Rats were placed on a wire mesh platform, and the filaments (2.0 g) were applied vertically to an area of the dermatome of the back adjacent to the incision site, with just enough pressure to gently bend the filament. Following this type of brief tactile stimulation, the absence or presence of vocalizations and instances of the rat attacking the filament was recorded (Yu et al., 2013).

2.7. Histopathological analyses

After 6 weeks of behavioral testing, rats were deeply anesthetized with ketamine and xylazine (350–500 mg/kg and 30–50 mg/kg; Sigma-Aldrich) and perfused intracardially with normal saline (0.9% sodium chloride, pH 7.4; Sigma-Aldrich) followed by 4% paraformaldehyde

(PFA) in 0.1 M PB (pH 7.4; Sigma-Aldrich). After perfusion, spinal cords were excised, post fixed in 4% PFA overnight at 4 °C, dehydrated in 10, 20 and 30% sucrose in 0.1 M PB, and frozen in dry ice-isopentane (~ − 45 °C). A 2-cm segment of spinal cord tissue centered at the injury site was serially cryosectioned at 20 μm for morphometric and mechanistic analyses.

Solvent blue and hematoxylin stain was done for tissue sections obtained from the lesion epicenter and 1, 2, 3, and 4 mm both rostral and caudal to the epicenter. The results were analyzed to measure averaged and summed group lesion volume and white matter (WM) sparing quantity as previously described (Teng et al., 2004; Ropper et al., 2017). For neuronal protection assessment, average surviving interneurons (INs) per 20 μm tissue in the intermediate gray matter (i.e., Rexed laminae V-VII) were quantified (Teng et al., 1998). To minimize miscounting only INs with proper soma size ($\Phi \geq 15$ μm) were included (red arrows, Fig. 3; Clarke et al., 1998). Smaller neurons ($\Phi < 6$ μm) were not countered (arrowheads, Fig. 3). Serial spinal cord sections from all study groups (i.e., the 1st 20 μm tissue section of each 200 μm spinal cord; total: 5 sections/1 mm spinal cord) were stained in blocks of all 4 groups. All morphological analyses were performed with the tissue recognized only by the animal number; the evaluator was blind to the treatment until the group summary of the data was completed.

2.8. Immunohistochemical (IHC) analysis

IHC assays for detecting inflammatory responses were done by using primary antibodies against glial fibrillary acidic protein (GFAP, 1:1000; Millipore), CD11b (1:250; AbD Serotec), and nitrotyrosine, a “fingerprint” of protein nitration (1:250, Santa Cruz). Angiogenesis signs were evaluated per immunoreactivity levels to primary antibodies against laminin (1:60, Sigma-Aldrich) and CD31 (1:400, Santa Cruz). To probe proliferation of endogenous neural stem cells (NSCs) a primary antibody against nestin (1:200; Santa Cruz) were used. Neurotrophic and anti-inflammation activities in the spinal cord were assessed by IHC reactivity to primary antibodies against brain-derived neurotrophic factor (BDNF, 1:250; Promega) and Interleukin 10 (IL-10, 1:250; Santa Cruz), respectively. Antibodies against mesoderm phenotypic lineage markers such as type I collagen (1:250; Santa Cruz), type II collagen (1:250; Santa Cruz), and alkaline phosphatase (1:250; Santa Cruz) were used to determinate donor hMSC fate (Thakor et al., 2018; Ropper et al., 2017). For evaluating signaling event of mechanotransduction, a primary antibody against Yes-associated protein (YAP) was used (1:200; Santa Cruz). Cell nuclei were counterstained with DAPI (Vectashield), and hMSC were tracked in the rat spinal cord through detecting IHC reactivity to primary antibodies against human CD90 (1:300; Santa Cruz) or human heat shock protein 27 (HSP27; 1:250, Stressgen Bioreagents). Serial spinal cord sections (i.e., the 1st 20 μm tissue section of each 200 μm spinal cord; total: 5 sections/1 mm spinal cord) of different levels were stained in blocks containing all 4 groups to permit the comparison of the targets post identical processing.

The following secondary antibodies were used in 1:250–300 dilutions: donkey anti-rabbit FITC, donkey anti-mouse Texas Red (TR), donkey anti-mouse FITC, donkey anti-goat Dylight 594, donkey anti-chicken TR, donkey anti-mouse FITC, and donkey anti-rabbit TR (all from Jackson Immunoresearch). Primary antibodies were incubated at 4 °C overnight, followed by secondary antibody incubation at room temperature for 1 h. Blocking was performed for 1 h at room temperature immediately before primary antibody incubation with the solution containing 3–5% bovine serum albumin (BSA; Invitrogen), 0.1% Triton X-100, and 0.05% Tween 20 (Sigma-Aldrich).

Imaging was performed using a Zeiss Axiovert 200 microscope equipped with an Axiocam CCD camera (Zeiss) or a Zeiss LSM1 confocal microscope equipped with Zeiss Zen 2011 software set (Carl Zeiss Microimaging), with appropriate filters for FITC, Texas Red, and DAPI. The immunoreactivity was semi-quantified by first measuring the signal intensity above a threshold level that avoids non-specific reactivity; then, dividing the number of pixels above the intensity threshold by the total pixel count of the view field to yield relative signal values for the quantity of a particular antigen in a selected region (Teng et al., 2004; Thakor et al., 2018).

2.9. Statistics

The group size (n = 7) was decided based on our previously published work to obtain sufficient statistical power to evaluate neuroprotection outcomes following lower thoracic SCI in rats (Teng et al., 1998). All statistical analyses were computed through using SPSS software version 19 (IBM Corp, Somers, NY, USA). One-way or two-way analysis of variance (ANOVA) with or without repeated measures was used to assess differences in behavioral, histology, and IHC data among the 4 experimental groups; for specific intergroup comparisons, Tukey's *post-hoc* test was performed. For categorical data comparison, Fisher's exact test was used. In all cases, $P < 0.05$ was considered to be statistically significant (Teng et al., 2002).

3. Results

3.1. Biophysical features of the PLGA scaffolds

In corroboration for our hypothesis, the compressibility of the scaffolds indeed increased as the PLGA concentration decreased (Fig. 1C). Specifically, when compressed with a force of 75 g from an aneurysm clip (Fig. 1B_4), the 40% PLGA scaffold on average maintained about 80% of its original width, whereas the 20% and 10% PLGA scaffolds were compressed to about 46% and 33% of their original width, respectively (n = 5/group; Fig. 1C). The data suggested that the reduced concentration of PLGA in the casting solution might have also resulted in a lower amount of PLGA between the salt crystals after casting, thus increasing the softness and deformability of the scaffolds.

To further investigate whether the texture of a scaffold with a given PLGA concentration could be physicochemically manipulated, we synthesized some relatively “stiff” scaffolds made of 40% PLGA and examined if UV irradiation or NaOH treatment could “soften” them (Fig. 1B_2-4). UV irradiation for 2 h triggered a notable increase in group average compressibility under a 75 g force, from about 39% compression (i.e., ~61% of its original width) to ~65% compression (i.e., ~35% of its original width); there was a further increase to ~75% group mean compression rate following UV irradiation for 5 h (i.e., ~25% of its original width; Fig. 1D). For this particular assay, no further increases in compressibility were observed with UV irradiation that lasted for 8 or 22 h (data not shown). However, after UV irradiation, the scaffolds became crumbly and disintegrated easily, and they degraded quickly when exposed to cell culture medium. Lastly, treatment with NaOH exposure for 25 min at concentrations of 0.1 and 1.0 M also increased the compressibility of the scaffolds, although the magnitude of the increase was less than that observed when decreasing the PLGA concentration (data not shown).

Based on these findings, we decided to use 40% and 10% PLGA for the stiffer and softer scaffolds, respectively, without UV or NaOH preconditioning in subsequent experiments. The results demonstrated that manipulation of the PLGA concentration was both readily to implement and reliable for maintaining the scaffold integrity.

3.2. Evaluations of coordinated hindlimb motor functions

To test the hypothesis that degrees of scaffold stiffness might affect functional multipotency and fate of hMSCs in the implant to influence recovery process after SCI, hindlimb locomotion, inclined plane, and spinal reflex data were analyzed. Importantly, the average BBB score of the affected hindlimb in SCI rats treated with soft PLGA-scaffolded hMSCs was significantly higher ($P < 0.05$) compared to that of the

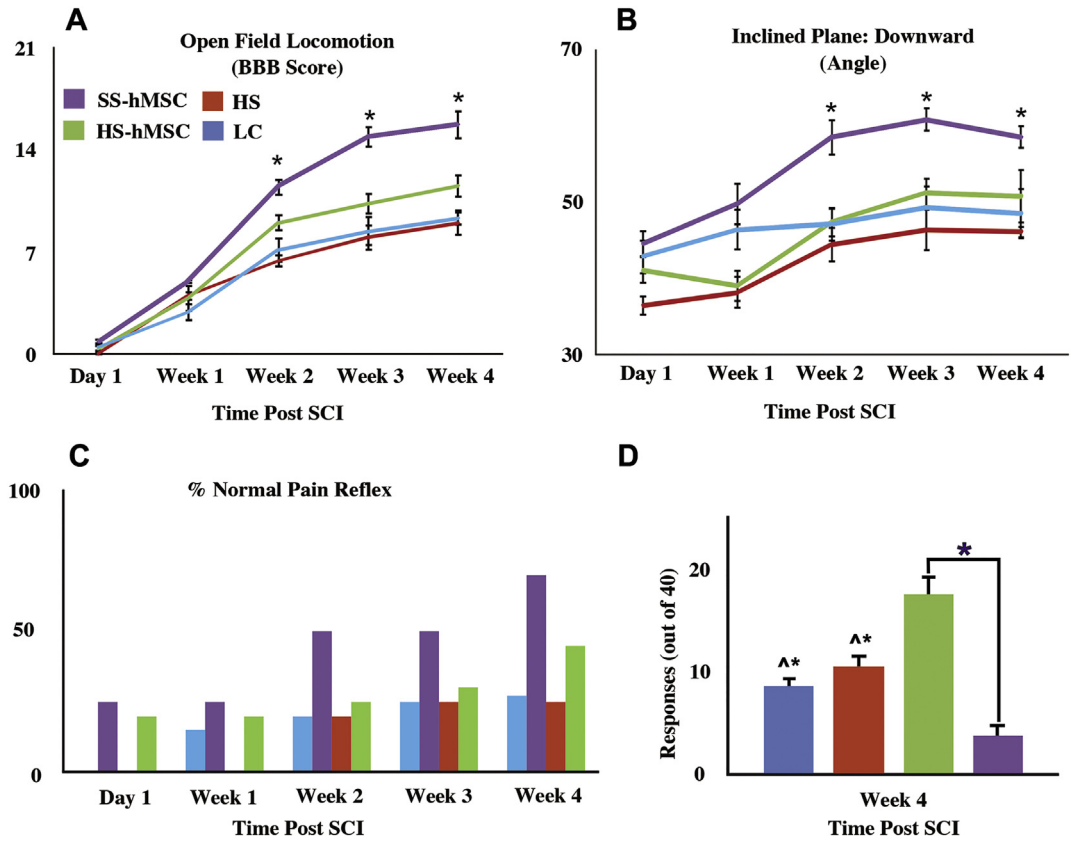

Fig. 2. Behavioral assessments of functional recovery. A. Group average BBB open-field locomotion scores of the lesion side hind limbs. The average score of improvement for SCI rats treated with soft PLGA-scaffolded hMSCs (SS-hMSC) was significantly higher than that of the hard scaffold-hMSC (HS-hMSC), hard scaffold (HS) or lesion only control (LC) group, starting 14 days post SCI (note: there was no any significant differences between the control groups; *, $P < 0.05$, two-way ANOVA with repeated measures and Tukey's post hoc test; n = 7/group). (B) Inclined plane test with rats facing downward. SCI rats receiving implantation of soft PLGA-scaffolded hMSCs, on average, maintained body stability significantly better than the controls that showed similar poor performances (*, $P < 0.05$, two-way ANOVA with repeated measures and Tukey's post hoc test; n = 7/group). (C) Percentage of SCI rats in each group with a normal spinal cord reflex in response to the toe pinching/pain test. The soft PLGA-hMSC group had the highest average % of normal range pain reflex compared to all controls. By 4 weeks after SCI, about 75% rats in the soft PLGA-hMSC group showed normal response to a brief tow pinch relative to 40%, 22% and 20% in the hard PLGA-hMSC, lesion only, and hard PLGA group, respectively. (D) At-level allodynia test. At-level allodynia condition was assessed by applying a standard 2 g Semmes-Weinstein monofilament test in the dermatome of T9–10. The average number of avoidance response was significantly decreased in SCI rats that were transplanted with the soft PLGA-scaffolded hMSCs, compared to control groups. The hard scaffold alone and lesion only groups on average also had significantly less hypersensitive responses than the hard PLGA-hMSC group (* vs. soft PLGA-hMSC group; ^ vs. hard PLGA-hMSC group; $P < 0.05$, Fisher's exact test; n = 7/group; note: missing of group mean value bar indicated 0% of normal response).

group treated with hard PLGA-scaffolded hMSCs, hard scaffold alone, or no implant throughout the 4-weeks of evaluation (Fig. 2A).

To further determine changes in hindlimb coordinated functions, animals were tested facing upward and downward on an inclined plane. In the upward orientation, all groups exhibited statistically similar performance (data not shown), which suggested that the rats had similar forelimb strength and general wellbeing condition (Choi et al., 2005). Notably, in the downward-facing setting the group that received soft PLGA-scaffolded hMSCs showed significantly improved performance starting 7 days post SCI, compared to all 3 other groups (Fig. 2B). However, there were no discernible differences in group average BBB score or mean incline plane angle at any time point evaluated between SCI rats that received hard PLGA-scaffolded hMSCs, hard PLGA scaffold alone, or lesion only (Fig. 2A and B).

3.3. Tests of spinal reflexes and nociception

Examinations of spinal cord sensory reflexes revealed significantly improved recovery in responses to a brief hindlimb toe pinch in the group that received soft PLGA-scaffolded hMSCs, relative to SCI rats with hard PLGA-scaffolded hMSCs, hard scaffold alone, or no implant. At 4 weeks post SCI, about 75% of SCI rats treated with soft PLGA + hMSCs regained a normal nociceptive withdrawal reflex in the hindlimb on the ipsilesional side in contrast to ~40% in the group that received treatment of hard PLGA-scaffolded hMSCs, and ~22% and ~20% of SCI rats with no implant or hard scaffold alone, respectively (Fig. 2C). The outcomes suggested that hMSCs interacted with soft PLGA scaffold beneficially to enhance their combinatorial therapeutic effect (see below for details; Thakor et al., 2018; Ropper et al., 2017). Contrariwise, hard PLGA scaffolds, despite housing ~3 times more hMSCs per unit than soft scaffolds, appeared to negatively affect neural repair potentials of hMSCs and host healing process, triggering behavioral outcomes similar to those of SCI rats that were transplanted with hard scaffold only (Fig. 2A and C).

To more precisely evaluate the impact of the varied treatments on neuropathic pain evolvement after SCI, Semmes-Weinstein filament test (2 g) was applied to determine at-level allodynia at 4 weeks following SCI. SCI rats implanted with soft PLGA-scaffolded hMSCs demonstrated the lowest group average response rate relative to all other groups that showed significantly higher prevalence of hypersensitivity (Fig. 2D). Overall, the data suggested that high rigidity scaffolds unfavorably influenced therapeutic capability of donor hMSCs as well as host spinal cord's healing capability, resulting in no significant improvement in all functional parameters evaluated (Fig. 2A–C) and further worsened at

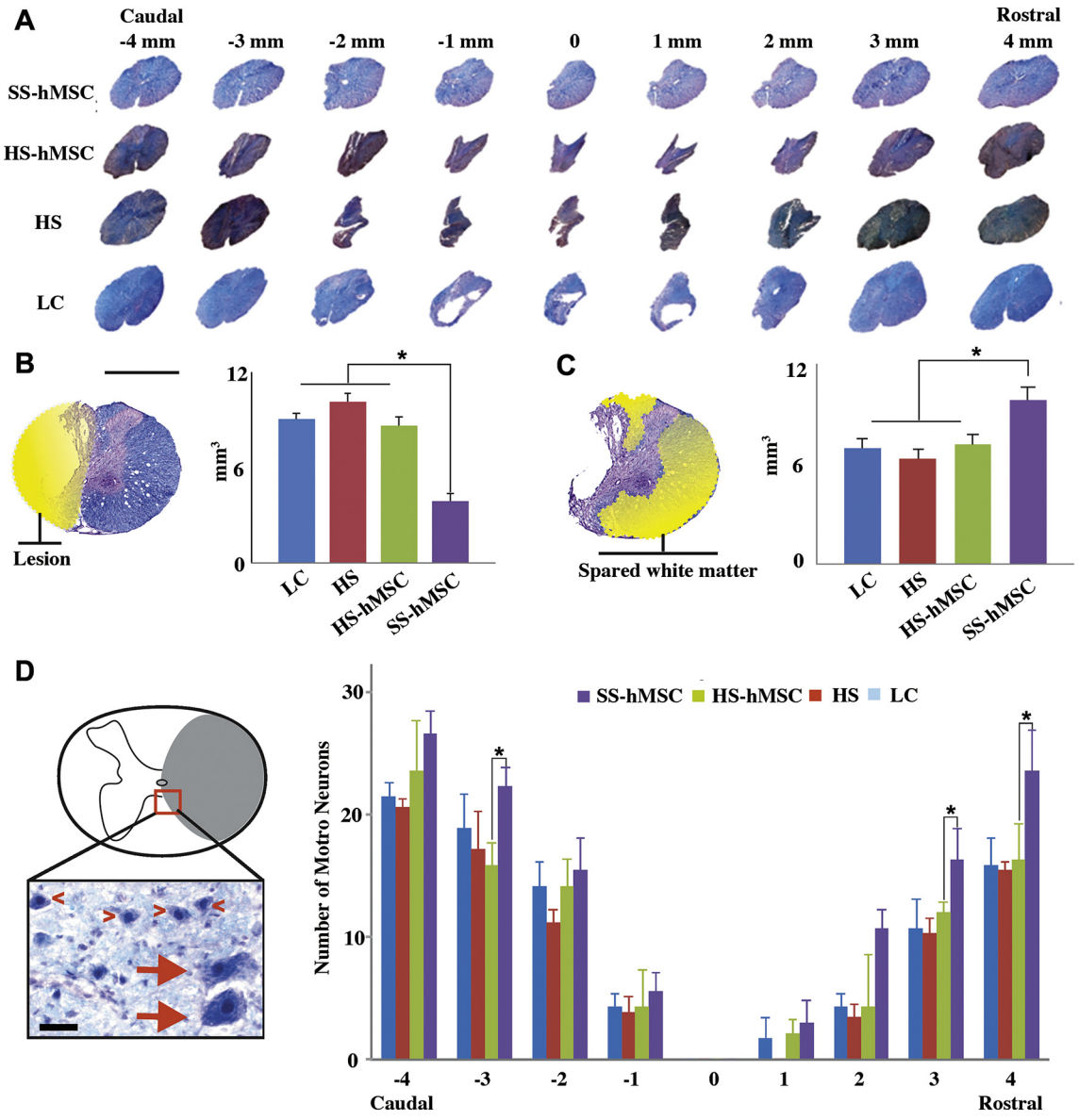

Fig. 3. Histopathological analyses. A. Profiling of cross sections from a representative spinal cord of each group. Solvent blue and hematoxylin-stained serial 20 μm transverse spinal cord sections at and around the injury epicenter (in 1 mm increments) showed that the soft PLGA-hMSC group (SS-hMSC) had the highest degree of tissue preservation, compared to hard PLGA-scaffolded hMSCs (HS-hMSC), hard PLGA alone (HS), and lesion only control (LC) groups. B. Morphometry-based measurement of the lesion volume. Spinal cords implanted with the soft PLGA-scaffolded hMSCs exhibited the smallest group average lesion volume compared to all 3 control groups (*, $P < 0.05$, one-way ANOVA with Tukey's post hoc test; n = 7/group; lesion area was colored yellow; scale bar: 1 mm). C. Quantification of white matter (WM) sparing around the epicenter. No significant difference was detected between the 3 control groups for mean MW preservation amount that was very low. In contrast, the soft PLGA-hMSC group had a significantly higher mean volume of WM sparing (*, $P < 0.05$, one-way ANOVA with Tukey's post hoc test; n = 7/group; spared WM area was colored yellow). D. Epicenter region interneuron (IN) protection. Quantitative assessment of spinal cords of each group determined that the implantation of the soft PLGA-scaffolded hMSCs significantly preserved average IN numbers per 20 μm tissue section in Rexed laminae V-VII, relative to the controls at loci 3 and 4 mm rostral to the epicenter. The treatment also significantly spared INs on spinal cord level 3 mm caudal to the lesion site compared to the hard PLGA- hMSC group (*, $P < 0.05$, two-way ANOVA with repeated measures and Tukey's post hoc test; n = 7/group; scale bar: 15 μm). Note: only INs with proper soma size were countered (red arrows). Smaller neurons were not included (arrowheads; see Methods for more details). (For interpretation of the references to colour in this figure legend, the reader is referred to the web version of this article.)

level hypersensitivity relative to other groups (Fig. 2D).

3.4. Histopathological results

The SCI lesion volume consists of the primary syrinx, additional smaller cavities, and a loose web of connective tissue-like non-neural cells with their ECMs (Teng et al., 1999; Teng et al., 2002, 2004). Thus, it represents parenchymal regions with maximum amount of tissue loss. To measure the lesion volume, the injury areas were outlined in solvent blue/hematoxylin-stained spinal cord sections sampled at the hemisection epicenter and loci up to 4 mm both rostral and caudal away from it in 1 mm increments. The overall cross-section profile of the hMSC-seeded soft scaffold-treated spinal cords appeared to be best preserved, relative to the 3 other groups (Fig. 3A). Quantitative analysis showed that spinal cords receiving soft PLGA-scaffolded hMSCs had the least amount of tissue loss as exampled by the smallest group average lesion volume (Fig. 3B) and the highest group average level of WM preservation (Fig. 3C), relative to the control groups. Noticeably, spinal cords implanted with hard scaffold alone or hard PLGA-scaffolded hMSCs manifested the worst tissue loss at the epicenter region,

exhibiting further deterioration compared to the lesion only group (Fig. 3A).

To determine the neuronal effector that benefited from the treatment, the number of healthy-appearing INs in Rexed Laminae V-VII of the spinal cord cross section (thickness: 20 μm) was counted per an unbiased method reported before (i.e., discernible nuclear envelope and nucleolus: inset in Fig. 3D; Teng et al., 1998; Hadi et al., 2000). The average numbers of surviving INs at loci 3 and 4 mm rostral to the epicenter were significantly higher in the group that was transplanted with soft PLGA-scaffolded hMSCs than those of the spinal cords treated with hard PLGA-scaffolded hMSCs, hard scaffold alone, or no implant (Fig. 3D). The IN sparing effect of soft PLGA-scaffolded hMSCs was also significant on spinal cord level 3 mm caudal to the lesion site, relative to that of the hard PLGA-scaffolded hMSC group. Lastly, at the end of the study (i.e., ~6–8 weeks post SCI) both soft and hard scaffolds appeared to be totally degraded in the spinal cord (Teng et al., 2002; Yu et al., 2009; Ropper et al., 2017), indicating that the degradation speed was largely determined by the ratio of lactic acid in PLGA, not polymer rigidity as reported before (Makadia and Siegel, 2011).

3.5. IHC data

We observed long surviving donor cells only in the spinal cords treated with soft PLGA-scaffolded hMSCs per IHC reactivity to antibody against the 70-kilodalton heat shock proteins (i.e., HSP70). Similar to data reported before (Ropper et al., 2017), there were 2–3% of initially scaffolded hMSCs remaining detectable by ~6–8 weeks post SCI. To probe the anti-inflammatory effect of the treatment, expression profile of typical inflammatory markers around the injury epicenter was systematically evaluated. In corroboration to outcomes of tissue sparing (see above), compared to the spinal cords treated with soft PLGA-scaffolded hMSCs, there was much heightened production of neural inflammatory markers of CD11b (a marker of inflammatory cells including microglia, macrophages, natural killer cells, etc.), nitrotyrosine (a marker of oxidative protein nitration), and GFAP (a marker of reactive gliosis) on spinal cord level 3 mm caudal to the epicenter in groups that received hard PLGA-scaffolded hMSCs, hard scaffold alone or no implant (Fig. 4). The data suggested higher level presence of inflammatory cells, oxidative protein nitration, and reactive gliosis, respectively, in all 3 control groups (Fig. 4; Yu et al., 2009). The results indicated that hard PLGA as scaffolds diminished the anti-inflammatory and anti-oxidative properties of hMSCs (Thakor et al., 2018).

In order to determine major therapeutic effects of the implant, we first obtained coronal sections from the spinal cord segment 3 mm rostral to the epicenter for IHC staining of CD31, a marker of angiogenesis. It was known that hMSC treatment could induce formation of new blood vessels in target tissues (Ropper et al., 2017; Cortez-Toledo et al., 2019). Compared to lesion only and hard scaffold control groups, spinal cords receiving implantation of soft or hard PLGA-scaffolded hMSCs had significantly higher group average level of CD31 immunoreactivity, suggesting that they had stronger angiogenic activities (Fig. 5A).

Owing to their functional multipotency (Teng, 2019a; Thakor et al., 2018), donor hMSCs, in their stemness retention state, could induce host endogenous neurogenesis (Ropper et al., 2017). Therefore, the immunoreactivity of nestin, a NSC marker, in spinal cord sections 2 mm rostral to the injury epicenter was evaluated for neurogenic signs. There was a significantly elevated group mean level of nestin immunoreactivity in spinal cords implanted with soft PLGA-scaffolded hMSCs, compared to that from each of the 3 control groups (Fig. 5B). Moreover, group mean nestin IHC reactivity of spinal cords treated with hard PLGA-scaffolded hMSCs was significantly higher than that of hard scaffold alone or no implant group, suggesting that both angiogenic and neurogenic effects were derived from hMSCs (Fig. 5A and B).

Neural trophic factors and other cytokines are secreted by stem or progenitor cells including MSCs and NSCs that act as mediators of homeostasis for the surrounding environment (Teng et al., 2011; Teng, 2019a). Therefore, the immunoreactivities to BDNF, a neurotrophin and IL-10, an anti-inflammation cytokine were assessed in tissue section 1 mm caudal to the injury epicenter. More cells expressing BDNF (Fig. 5C: red) and IL-10 (Fig. 5C: green) were found in spinal cords that received soft PLGA-scaffolded hMSCs than those treated with hard PLGA-scaffolded hMSCs. No definitive immunoreactive signals of BDNF or IL-10 were found in the same region for lesion only and hard scaffold control groups (data not shown).

To analyze post-transplantation fate of hMSCs, IHC assays were done to detect immunosignals of alkaline phosphatase (an enzyme for osteogenesis; Baudry et al., 2019), collagen I (a component of tendons, ligaments, muscles, and bones), and collagen II (a component of articular cartilage and hyaline cartilage; Deshmukh et al., 2016), molecules that indicate presence of mesoderm lineage cell differentiations (Thakor et al., 2018). Cells with such markers are normally absent from the adult spinal cord (Ropper et al., 2017). Indeed, only spinal cord implanted with hard PLGA-scaffolded hMSCs showed high immunoreactivity to alkaline phosphatase and collagen II (Fig. 5D), as well as collagens I and II (Fig. 5E and D). The data suggested that donor hMSCs under direct scaffolding of hard PLGA were induced to differentiate towards mesoderm phenotypes such as bone, articular cartilage (e.g., production of alkaline phosphatase and type II collagen, respectively; Fig. 5D), and peripheral tissues expressing type I collagen (Fig. 5E). However, the increased immunoreactivity to collagen type IV (Fig. 5E), a major basal membrane component was found in spinal cords implanted with either hard or soft PLGA-scaffolded hMSCs, corroborating the augmented angiogenic signal seen in the same groups (Fig. 5A; Marchand et al., 2019).

We next investigated whether there was hMSC nuclear expression of YAP, a transcriptional co-activator and effector of the mechanosensitive Hippo pathway (Zhubanchaliyev et al., 2016). The results demonstrated that only hMSCs scaffolded by hard/high rigidity PLGA polymer exhibited nuclear YAP/TAZ immunoreactivity; in contrast, hMSCs seeded in soft PLGA scaffolds showed YAP/TAZ immunostain predominantly in the cytoplasm (Fig. 5F). The outcome confirmed that only the hard scaffold was capable to ignite mechanotransduction signaling of hMSCs, which was consistent with data obtained from IHC assay of mesodermal lineage differentiations.

4. Discussion

The present study elucidated that there were reciprocal interactions between the physical rigidity of PLGA scaffolds, seeded hMSCs, and injured spinal cords. Such communications influenced retention or loss of hMSC stemness function (e.g., production of trophic and anti-inflammatory factors, induction of endogenous NSC proliferation, etc.), ectopic mesodermal lineage differentiation, and spinal cord post-injury responses (e.g., inflammation, reactive gliosis, tissue preservation, neural restoration, etc.). In general, the findings suggested that low/soft rigidity PLGA scaffolding for hMSCs was crucial for the implant to orchestrate functional recovery in the injured adult rat spinal cord. Conversely, the high rigidity/hard PLGA-composed implant was detrimental for neural repair as it triggered loss of functional multipotency of donor cells, ectopic differentiation of mesodermal lineages, exacerbated host tissue damage, and no significant behavioral improvement in SCI rats.

We and our collaborators pioneered the platform technology of 3D polymer scaffolding that topologically mimicked a healthy spinal cord to deliver NSCs (Teng et al., 2002) for SCI. The approach effectively overcame a formidable barrier to investigating or developing cell therapies for neurotrauma due to no or extremely poor survival of stem cells transplanted in suspension inside severe, penetrating or open wounds of the central nervous system (CNS; Teng et al., 2002, 2018). We also investigated benefits of designing polymer-NSC implants that emulated the anatomical structure of the brain (Park et al., 2002) or

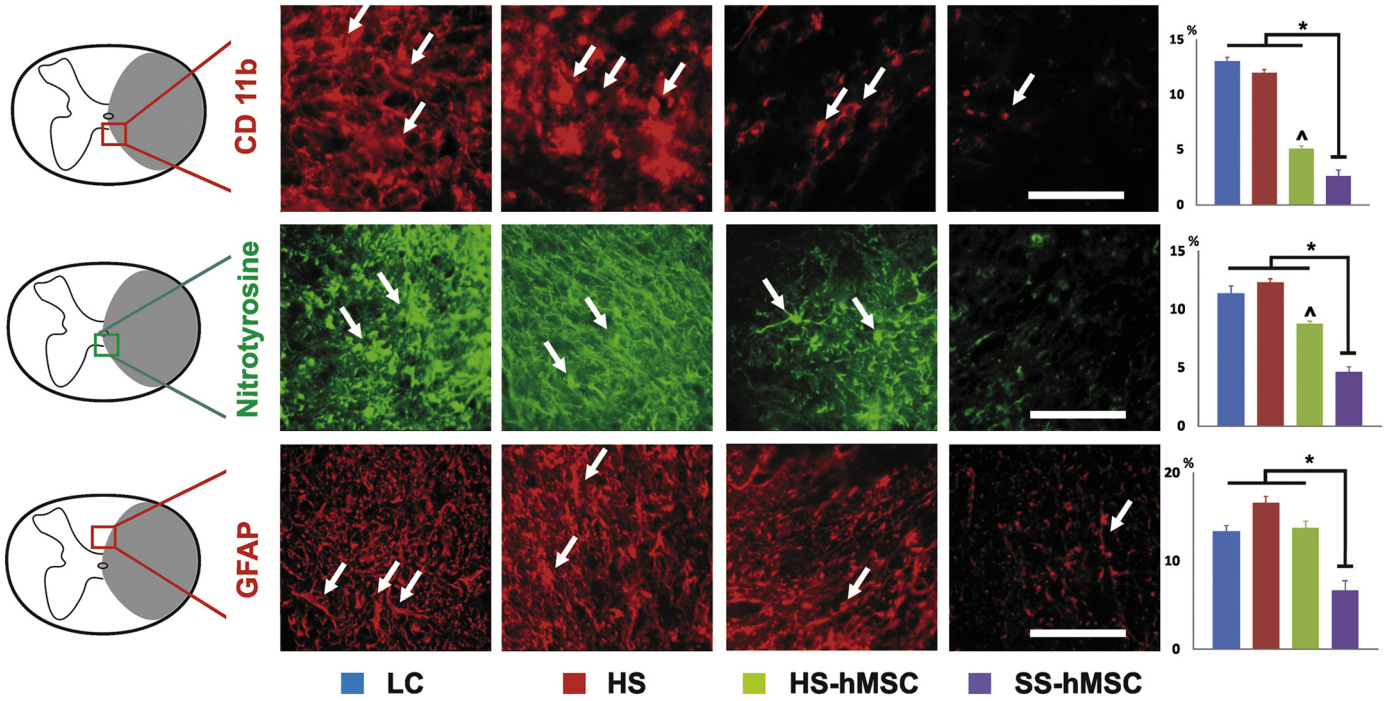

Fig. 4. Immunohistochemical evaluation of neural inflammation. A. Immunosteins of CD 11b, nitrotyrosine and GFAP (glial fibrillary acidic protein). Transverse spinal cord sections, 3 mm caudal to the injury epicenters in each group (one 20 μm section/200 μm tissue; signal levels in 5 sections/mm spinal cord were averaged for the mean value of one rat; n = 7/group), were immunohistochemically stained for CD 11b (a maker of inflammatory cells including monocytes, macrophages, microglia, and natural killer cells), nitrotyrosine (a protein nitration "fingerprint" for oxidative damage), and GFAP (a marker of reactive astrogliosis). Compared to hard PLGA-scaffolded hMSCs (HS-hMSC), hard scaffold (HS) and lesion only control (LC) groups, implantation of soft PLGA-hMSCs (SS-hMSC) significantly reduced group mean immunoreactivity to CD 11b, nitrotyrosine, and GFAP. Spinal cords of HS-hMSC group also showed significantly impeded neuroinflammatory responses relative to LC and HS groups (*, $P < 0.05$, one-way ANOVA with Tukey's post hoc test; scale bar: 100 μm). Note: Arrow-pointed target objects showed varied IHC profiles in different groups.

varied topological features as niches to induce neuronal differentiation (Jia et al., 2014), and embedding drugs for controlled release to protect donor cells (Yu et al., 2009).

The NSC or MSC-derived therapeutic events, which do not rely on direct neural cell replacement, were first validated for neural recovery post SCI (Teng et al., 2002; Kim et al., 2009; Myers et al., 2011; O'Shea et al., 2017; Teng et al., 2018). Thus, relative to the conventional view that is primarily concentrated on the totipotency, pluripotentcy and multipotency of cell lineage differentiation, accumulated data promoted us and our colleagues to establish Functional Multipotency of Stem Cells as a biological concept (Teng, 2019a). It describes the innate capability of the stem cell to exert interactive functions (e.g., production of trophic factors, cytokines, exosomes, formation of gap junctions, etc.) triggered by environmental cues to mediate homeostasis for proper cell division, migration, differentiation, organogenesis as well as system formation and function (Teng et al., 2008, 2011; Teng, 2019a). Following this reasoning, a broader range of stemness-enabled signaling, epigenetic and genetic endeavors have been uncovered. Our current data again confirms that it is crucial to invent multimodal biomaterials with features that can sustain such inducible multiple biofunctions of stem cells.

We recently reported that the hMSC's multiple functions (e.g., tropic factor secretion, anti-inflammation, immunoregulation, neuroprotection, and neurogenic and angiogenic effect) could be maintained by soft PLGA scaffolding; implantation of the construct markedly promoted neural recovery in the same model of SCI (Ropper et al., 2017). The treatment provided comprehensive impacts to galvanize the four essential events of Recovery Neurobiology (i.e., propriospinal network function, serotonergic reinnervation, neuromuscular junction integrity, and reanimation of locomotor pattern generator) of the injured adult rat spinal cord (Teng, 2019b; Ropper et al., 2017). We have now reconfirmed that the approach significantly protected neurons in Rexed Laminae V-VII, a fraction of which were propriospinal INs (Fig. 3). Indeed, there were discernibly more WM and less lesion volume in the spinal cord treated with soft PLGA-scaffolded hMSCs, comparing to all 3 control groups (Fig. 2). The therapeutic benefits were linked with the anti-inflammatory, angiogenic and neurogenic capabilities of hMSCs scaffolded by soft PLGA (Figs. 3-5). Because the scales of functional recoveries post the same type of treatment with soft PLGA-scaffolded hMSCs were replicated in the present study, we did not repeat neural tracing analyses performed by Ropper et al. (2017) or ex vivo assays by Thakor et al. (2018). However, future studies may verify possible optimizing effect of feeder cells (e.g., release of cytokines, etc.) on therapeutic potential of hMSCs during seeding onto soft scaffolds.

Interestingly, the lack of therapeutic impact of hard PLGA-scaffolded hMSCs did not appear to be linked with acute donor cell death but rather the loss of stemness plus ectopic differentiation of donor cells towards osteogenesis, chondrogenesis and myogenesis (Fig. 4 and Fig. 5; Dupont et al., 2011; Engler et al., 2006). The fate changes of hMSCs might have made cell seeding easier in the hard scaffold (e.g., ~3× more cells/per hard scaffold than a soft scaffold) as physical stresses often trigger cell clustering (Teng et al., 2018). For the spinal cord that is an ectoderm organ, such post-implantation development of hMSCs is detrimental due to its non-compatibility for the CNS (Goritz et al., 2011). The in vivo IHC data revealed that YAP immunoreactivity was within the nuclei of the hMSCs seeded in hard PLGA, but it was mostly within the cytoplasm of hMSCs scaffolded by soft PLGA. The outcome, in line with a previous report (Dupont et al., 2011), suggested that the expression of alkaline phosphatase, an osteogenic marker in hMSCs might be partially caused by YAP nuclear relocation following mechanotransduction activated by physical impact of hard PLGA scaffolding (Fig. 5E; Tang and Weiss, 2017; Wrighton, 2011; Totaro et al.,

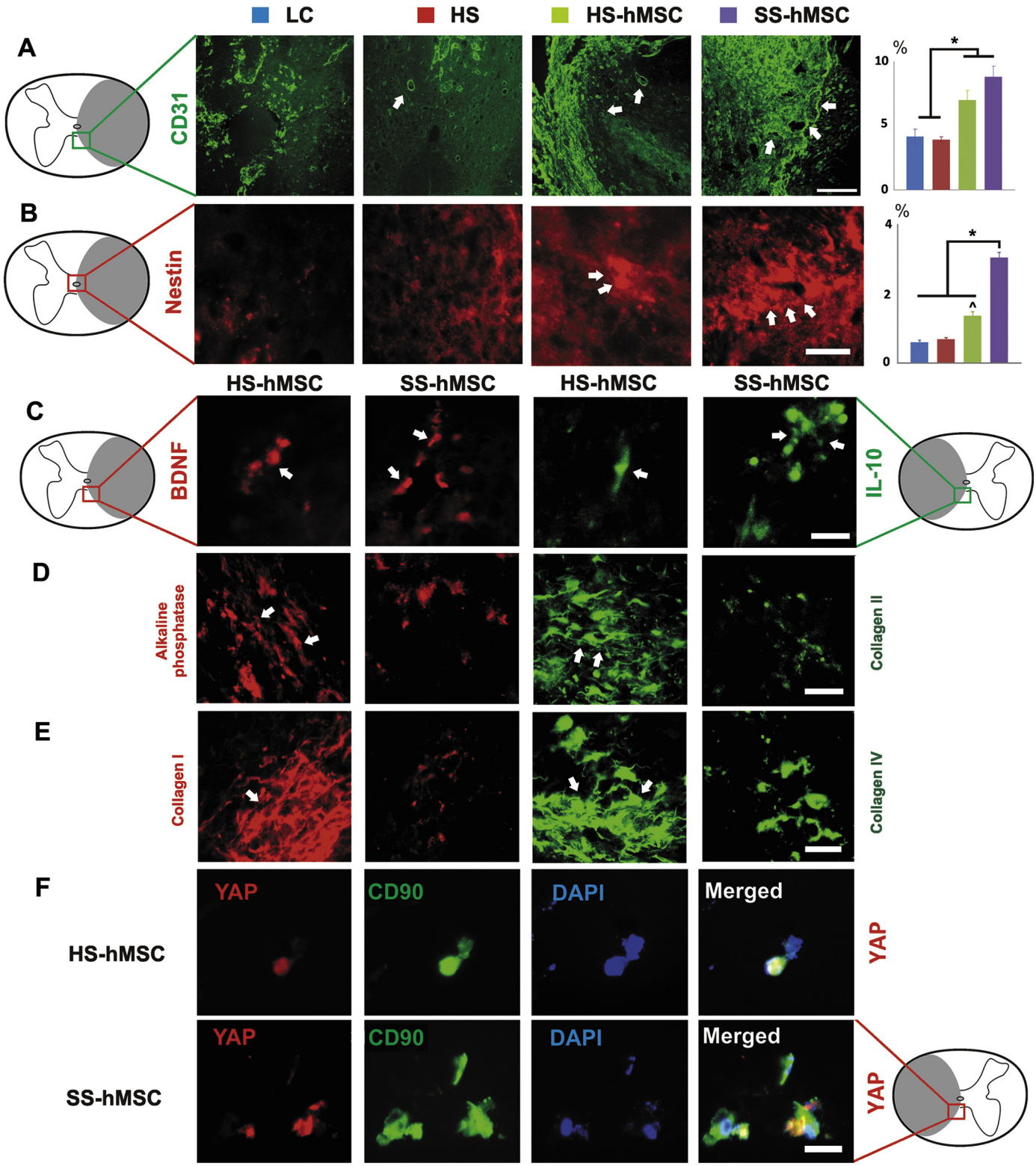

(caption on next page)

2018).

It was shown that MSCs seeded in polyacrylamide gels with varying bis-acrylamide crosslinking densities intended to increase osteogenic differentiation when interacting with stiffer matrices (Dupont et al., 2011). In fact, MSCs could specify their lineage differentiation based on the physical properties of the scaffolds they grow on. The cells can sense elasticity of the scaffold (i.e., the matrix stiffness that is a function of material rigidity) intracellularly via consequent tension changes of the actomyosin cytoskeletons following different pulling forces exerted from the matrix (Smith et al., 2017; Jaalouk and Lammerding, 2009; Discher et al., 2005). Therefore, it is utterly important for the field to understand how biophysical design of a particular polymer scaffold can affect the function and fate of the seeded stem cell, modifying the therapeutic impact of the implant. Such knowledge and technology will

Fig. 5. Analysis of neural repair mechanisms. A. Representative images of immunohistochemical (IHC) stain using antibodies against CD31 (i.e., platelet/endothelial cell adhesion molecule-1, an angiogenesis marker). Treatment with either soft or hard PLGA-scaffolded hMSCs (SS-hMSC or HS-hMSC) increased angiogenic immunoreactivity in tissues 3 mm rostral to the epicenter, compared to lesion only (LC) and hard scaffold alone (HS) groups (*, $P < 0.05$, one-way ANOVA with Tukey's post hoc test; scale bar: 200 μm; tissue sampling method per Fig. 4). B. Activation of endogenous neural stem cells (NSCs) was determined by presence of nestin immunoreactivity, a NSC marker in the spinal cord (tissue level: 2 mm rostral to the epicenter; sampling method per A). There was a significantly higher average level of nestin immunoreactivity in spinal cords implanted with soft PLGA-scaffolded hMSCs, relative to all 3 control groups. The group average immunoreactivity level of nestin in spinal cords of SS-hMSC group was also discernibly higher than LC and HS groups (*, $P < 0.05$, one-way ANOVA with Tukey's post hoc test; $n = 7$/group; scale bar: 50 μm). C. Compared to spinal cords in LC and HS groups that showed no presence of BDNF (brain derived neurotrophic factor, a neurotrophin) and IL-10 (interleukin 10, an anti-inflammatory cytokine; data not shown), transplantation of soft PLGA-scaffolded hMSCs triggered detectible immunoreactivity to BDNF (red in left panels) and IL-10 (green in right panels). Less signal scales of the two factors were found in spinal cords implanted with hard scaffold-hMSCs (scale bar: 50 μm; level of tissue sections: 1 mm caudal to the epicenter; sampling method per A). D and E. Representative images of the spinal cord (tissue sampling per C) showed that transplantation of hard scaffold-hMSCs resulted in expression of alkaline phosphatase, an osteogenesis marker and collagen II, a primary extracellular matrix molecule in articular cartilage in the spinal cord (D), whereas areas of such immunoreactivities were much scattered or negligible in SS-hMSC group and no such signals existed in LC and HS groups that did not receive any hMSC (data not shown). Similar results were obtained for immunoreactivities to collagens I (the most abundant collagen in peripheral tissues of the bone, tendon, ligament, dermis, scar, etc.); however, either soft or hard scaffold-hMSC treatment increased immunoreactivity to collagen IV (a primary collagen in the basal lamina), with soft scaffold-hMSCs being more effective (E), suggesting that the angiogenic effect of hMSCs was better preserved by the soft scaffold as observed in A (scale bars: 50 μm; tissue sampling per C). F. Representative images of YAP/TAZ immunoreactivity in a spinal cord section that was translocalized to the nucleus of a CD90 positive donor hMSC seeded in the hard PLGA scaffold (upper panel), but YAP/TAZ immunosignals remained in the cytoplasm of CD90 positive hMSCs seeded in the soft scaffold that were grafted into an injured spinal cord (lower panel; tissue sampling for C; scale bar: 8 μm). Note: Arrow-pointed target objects showed varied IHC profiles in different groups. (For interpretation of the references to colour in this figure legend, the reader is referred to the web version of this article.)

enable us to manufacture biomaterials to meet unique needs of specific organ or system (including the CNS) reconstruction.

In summary, the rigidity and stiffness of PLGA scaffolds can modulate functional multipotency and fate choice of hMSCs and host responses in vivo, affecting the extent of functional recovery in a rat model of SCI. Thus, fabrication of precisely designed polymer that meets specific demands of a particular tissue is crucial for target organ reconstitution (Hollister et al., 2002; Irvine and Venkatraman, 2016; Reighard et al., 2018). For injured adult mammalian spinal cords, soft and degradable polymer scaffolds are more supportive for donor hMSCs to jointly ignite pro-recovery responses from host cells and neural circuitry (Caliari et al., 2016; Ropper et al., 2017; Thakor et al., 2018). These features and their related specific signaling pathways should be further characterized in order to devise future clinical grade implants to treat neurotrauma.

Author contributions

I.B.H., D.K.T., A.E.R, D.Y., L.W., X.Z., S.W.K., and Y.D.T. performed the experiments and generated data. D.K.T. and Y.D.T. designed polymer methodology and completed Fig. 1. I.B.H., D.K.T., A.E.R., D.Y., L.W., S.W.K., X.Z., R.D.Z. and Y.D.T. analyzed the data. I.B.H., D.K.T., A.E.R., and Y.D.T. drafted the manuscript. Y.D.T. conceived, funded and supervised the study, and rewrote the paper.

Competing financial interests

The authors declare that they have no competing financial interests for the reported project.

Acknowledgement

This work was supported by CIMT-DoD, Teng Lab Research Fund, DoD-CDMRP-SCIRP and US Veterans Affairs Department's Rehabilitation R&D grants to Y.D.T., and a research fund to Y.D.T. & R.D.Z. at the Spaulding Rehabilitation Hospital from the Cele H. & William B. Rubin Family Fund, Inc. for the Gordon Program in Clinical Paralysis Research.

References

Bao, X., Wei, J., Feng, M., Lu, S., Li, G., Dou, W., Ma, W., Ma, S., An, Y., Qin, C., Zhao, R.C., Wang, R., 2011. Transplantation of human bone marrow-derived mesenchymal stem cells promotes behavioral recovery and endogenous neurogenesis after cerebral ischemia in rats. Brain Res. 1367, 103–113.

Baudry, A., Schneider, B., Launay, J.M., Kellermann, O., 2019. Serotonin in stem cell based-dental repair and bone formation: a review. Biochimie 161, 65–72 (pii: S0300-9084(18)30226–8).

Caliari, S.R., Vega, S.L., Kwon, M., Soulas, E.M., Burdick, J.A., 2016. Dimensionality and spreading influence MSC YAP/TAZ signaling in hydrogel environments. Biomaterials 103, 314–323.

Choi, H., Liao, W.L., Newton, K.M., Onario, R.C., King, A.M., Desilets, F.C., Woodard, E.J., Eichler, M.E., Frontera, W.R., Sabharwal, S., Teng, Y.D., 2005. Respiratory abnormalities resulting from midcervical spinal cord injury and their reversal by serotonin 1A agonists in conscious rats. J. Neurosci. 25, 4550–4559.

Cigognini, D., Satta, A., Colleoni, B., Silva, D., Donega, M., Antonini, S., Gelain, F., 2011. Evaluation of early and late effects into the acute spinal cord injury of an injectable functionalized self-assembling scaffold. PLoS ONE 6, e19782.

Clarke, H.A., Dekaban, G.A., Weaver, L.C., 1998. Identification of lamina V and VII interneurons presynaptic to adrenal sympathetic preganglionic neurons in rats using a recombinant herpes simplex virus type 1. Neuroscience 85, 863–872.

Colzani, B., Pandolfi, L., Hoti, A., Iovene, P.A., Natalello, A., Avvakumova, S., Colombo, M., Prosperi, D., 2018. Investigation of antitumor activities of trastuzumab delivered by PLGA nanoparticles. Int. J. Nanomedicine 13, 957–973.

Cortez-Toledo, E., Rose, M., Agu, E., Dahlenburg, H., Yao, W., Nolta, J.A., Zhou, P., 2019. Enhancing retention of human bone marrow mesenchymal stem cells with pro-survival factors promotes angiogenesis in a mouse model of limb ischemia. Stem Cells Dev. 28, 114–119.

Cyranoski, D., 2019. Japan's approval of stem-cell treatment for spinal-cord injury concerns scientists. Nature 565, 544–545.

Deshmukh, S.N., Dive, A.M., Moharil, R., Munde, P., 2016. Enigmatic insight into collagen. J. Oral Maxillofac. Pathol. 20, 276–283.

Discher, D.E., Janmey, P., Wang, Y.L., 2005. Tissue cells feel and respond to the stiffness of their substrate. Science 310, 1139–1143.

Dupont, S., Morsut, L., Aragona, M., Enzo, E., Giulitti, S., Cordenonsi, M., Zanconato, F., Le Digabel, J., Forcato, M., Bicciato, S., Elvassore, N., Piccolo, S., 2011. Role of YAP/TAZ in mechanotransduction. Nature 474, 179–183.

Engler, A.J., Sen, S., Sweeney, H.L., Discher, D.E., 2006. Matrix elasticity directs stem cell lineage specification. Cell 126, 677–689.

Goritz, C., Dias, D.O., Tomilin, N., Barbacid, M., Shupliakov, O., Frisen, J., 2011. A pericyte origin of spinal cord scar tissue. Science 333, 238–242.

Hadi, B., Zhang, Y.P., Burke, D.A., Shields, C.B., Magnuson, D.S., 2000. Lasting paraplegia caused by loss of lumbar spinal cord interneurons in rats: no direct correlation with motor neuron loss. J. Neurosurg. 93, 266–275.

Hejcl, A., Sedy, J., Kapcalova, M., Toro, D.A., Amemori, T., Lesny, P., Likavcanova-Masinova, K., Krumbholcova, E., Pradny, M., Michalek, J., Burian, M., Hajek, M., Jendelova, P., Sykova, E., 2010. HPMA-RGD hydrogels seeded with mesenchymal stem cells improve functional outcome in chronic spinal cord injury. Stem Cells Dev. 19, 1535–1546.

Hofstetter, C.P., Schwarz, E.J., Hess, D., Widenfalk, J., El Manira, A., Prockop, D.J., Olson, L., 2002. Marrow stromal cells form guiding strands in the injured spinal cord and promote recovery. Proc. Natl. Acad. Sci. U. S. A. 99, 2199–2204.

Hollister, S.J., Maddox, R.D., Taboas, J.M., 2002. Optimal design and fabrication of scaffolds to mimic tissue properties and satisfy biological constraints. Biomaterials 23, 4095–4103.

Hwang, D.H., Kim, H.M., Kang, Y.M., Joo, I.S., Cho, C.S., Yoon, B.W., Kim, S.U., Kim, B.G., 2011. Combination of multifaceted strategies to maximize the therapeutic benefits of neural stem cell transplantation for spinal cord repair. Cell Transplant. 20, 1361–1379.

Irvine, S.A., Venkatraman, S.S., 2016. Bioprinting and differentiation of stem cells. Molecules (Basel, Switzerland) 21 (pii: E1188).

Jaalouk, D.E., Lammerding, J., 2009. Mechanotransduction gone awry. Nat. Rev. Mol. Cell Biol. 10, 63–73.

Jia, C., Yu, D., Lamarre, M., Leopold, P.L., Teng, Y.D., Wang, H., 2014. Patterned

electrospun nanofiber matrices via localized dissolution: potential for guided tissue formation. Adv. Mater. 26, 8192–8197.
Kim, H.M., Hwang, D.H., Lee, J.E., Kim, S.U., Kim, B.G., 2009. Ex vivo VEGF delivery by neural stem cells enhances proliferation of glial progenitors, angiogenesis, and tissue sparing after spinal cord injury. PLoS ONE 4, e4987.
Kubinova, S., Horak, D., Hejcl, A., Plichta, Z., Kotek, J., Sykova, E., 2011. Highly superporous cholesterol-modified poly(2-hydroxyethyl methacrylate) scaffolds for spinal cord injury repair. J. Biomed. Mater. Res. Part A 99, 618–629.
Makadia, H.K., Siegel, S.J., 2011. Poly lactic-co-glycolic acid (PLGA) as biodegradable controlled drug delivery carrier. Polymers 3, 1377–1397.
Marchand, M., Monnot, C., Muller, L., Germain, S., 2019. Extracellular matrix scaffolding in angiogenesis and capillary homeostasis. Semin. Cell Dev. Biol. 89, 147–156.
Myers, S.A., DeVries, W.H., Andres, K.R., Gruenthal, M.J., Benton, R.L., Hoying, J.B., Hagg, T., Whittemore, S.R., 2011. CD47 knockout mice exhibit improved recovery from spinal cord injury. Neurobiol. Dis. 42, 21–34.
Oh, S.K., Choi, K.H., Yoo, J.Y., Kim, D.Y., Kim, S.J., Jeon, S.R., 2016. A phase III clinical trial showing limited efficacy of autologous mesenchymal stem cell therapy for spinal cord injury. Neurosurg. 78, 436–447.
Ohta, M., Suzuki, Y., Noda, T., Ejiri, Y., Dezawa, M., Kataoka, K., Chou, H., Ishikawa, N., Matsumoto, N., Iwashita, Y., Mizuta, E., Kuno, S., Ide, C., 2004. Bone marrow stromal cells infused into the cerebrospinal fluid promote functional recovery of the injured rat spinal cord with reduced cavity formation. Exp. Neurol. 187, 266–278.
O'Shea, T.M., Burda, J.E., Sofroniew, M.V., 2017. Cell biology of spinal cord injury and repair. J. Clin. Invest. 127, 3259–3270.
Papa, S., Vismara, I., Mariani, A., Barilani, M., Rimondo, S., De Paola, M., Panini, N., Erba, E., Mauri, E., Rossi, F., Forloni, G., Lazzari, L., Veglianese, P., 2018. Mesenchymal stem cells encapsulated into biomimetic hydrogel scaffold gradually release CCL2 chemokine in situ preserving cytoarchitecture and promoting functional recovery in spinal cord injury. J. Control. Release 278, 49–56.
Park, K.I., Teng, Y.D., Snyder, E.Y., 2002. The injured brain interacts reciprocally with neural stem cells supported by scaffolds to reconstitute lost tissue. Nat. Biotechnol. 20, 1111–1117.
Reighard, C.L., Hollister, S.J., Zopf, D.A., 2018. Auricular reconstruction from rib to 3D printing. J. 3D Print Med. 2, 35–41.
Ropper, A.E., Thakor, D.K., Han, I., Yu, D., Zeng, X., Anderson, J.E., Aljuboori, Z., Kim, S.W., Wang, H., Sidman, R.L., Zafonte, R.D., Teng, Y.D., 2017. Defining recovery neurobiology of injured spinal cord by synthetic matrix-assisted hMSC implantation. Proc. Natl. Acad. Sci. U. S. A. 114, E820–E829.
Smith, L., Cho, S., Discher, D.E., 2017. Mechanosensing of matrix by stem cells: from matrix heterogeneity, contractility, and the nucleus in pore-migration to cardiogenesis and muscle stem cells in vivo. Semin. Cell Dev. Biol. 71, 84–98.
Spejo, A.B., Chiarotto, G.B., Ferreira, A.D.F., Gomes, D.A., Ferreira Jr., R.S., Barraviera, B., Oliveira, A.L.R., 2018. Neuroprotection and immunomodulation following intraspinal axotomy of motoneurons by treatment with adult mesenchymal stem cells. J. Neuroinflammation 15, 230.
Tang, Y., Weiss, S.J., 2017. Snail/slug-YAP/TAZ complexes cooperatively regulate mesenchymal stem cell function and bone formation. Cell Cycle 16, 399–405.
Teng, Y.D., 2019a. Functional multipotency of stem cells and recovery neurobiology of injured spinal cord. Cell Transplant. 28, 963689719850088 (PMID: 31134830).
Teng, Y.D., 2019 Mar 13b. Functional multipotency of stem cells: biological traits gleaned from neural progeny studies. Semin. Cell Dev. Biol. https://doi.org/10.1016/j.semcdb.2019.02.002. (pii: S1084-9521(18)30059-4. (PMID:30822497) [Epub ahead of print].
Teng, Y.D., Mocchetti, I., Wrathall, J.R., 1998. Basic and acidic fibroblast growth factors protect spinal motor neurones in vivo after experimental spinal cord injury. Eur. J. Neurosci. 10, 798–802.
Teng, Y.D., Lavik, E.B., Qu, X., Park, K.I., Ourednik, J., Zurakowski, D., Langer, R., Snyder, E.Y., 2002. Functional recovery following traumatic spinal cord injury mediated by a unique polymer scaffold seeded with neural stem cells. Proc. Natl. Acad. Sci. U. S. A. 99, 3024–3029.
Teng, Y.D., Choi, H., Onario, R.C., Zhu, S., Desilets, F.C., Lan, S., Woodard, E.J., Snyder, E.Y., Eichler, M.E., Friedlander, R.M., 2004. Minocycline inhibits contusion-triggered mitochondrial cytochrome c release and mitigates functional deficits after spinal cord injury. Proc. Natl. Acad. Sci. U. S. A. 101, 3071–3076.
Teng, Y.D., Santos, F.N., Black, P.M., Konya, D., Park, K.I., Sidman, R.L., Snyder, E.Y., 2008. Neural stem cells: multipotency beyond self-renewal and phenotypic differentiation. In: Atala, A., Lanza, R., Thomson, J.A. (Eds.), Principles of Regenerative Medicine. Academic Press, Cambridge, pp. 300–317.
Teng, Y.D., Kabatas, S., Li, J., Wakeman, D.R., Snyder, E.Y., Sidman, R.L., 2010. Functional multipotency of neural stem cells and its therapeutic implications. In: Ulrich, H. (Ed.), Perspectives of Stem Cells: From Tools for Studying Mechanisms of Neuronal Differentiation towards Therapy. Springer Netherlands, Dordrecht, pp. 255–270.
Teng, Y.D., Yu, D., Ropper, A.E., Li, J., Kabatas, S., Wakeman, D.R., Wang, J., Sullivan, M.P., Redmond Jr., D.E., Langer, R., Snyder, E.Y., Sidman, R.L., 2011. Functional multipotency of stem cells: a conceptual review of neurotrophic factor-based evidence and its role in translational research. Curr. Neuropharmacol. 9, 574–585.
Teng, Y.D., Wang, L., Zeng, X., Wu, L., Toktas, Z., Kabatas, S., Zafonte, R.D., 2018. Updates on human neural stem cells: From generation, maintenance, and differentiation to applications in spinal cord injury research. In: Buzanska, L. (Ed.), Human Neural Stem Cells: From Generation to Differentiation and Application. Springer International Publishing, Cham, pp. 233–248.
Teng, Y.D., Mocchetti, I., Taveira-DaSilva, A.M., Gillis, R.A., Wrathall, J.R., 1999. Basic fibroblast growth factor increases long-term survival of spinal motor neurons and improves respiratory function after experimental spinal cord injury. J. Neurosci. 19, 7037–7047.
Thakor, D.K., Wang, L., Benedict, D., Kabatas, S., Zafonte, R.D., Teng, Y.D., 2018. Establishing an Organotypic system for investigating multimodal neural repair effects of human Mesenchymal stromal stem cells. Curr. Protoc. Stem Cell Biol. 47, e58.
Totaro, A., Panciera, T., Piccolo, S., 2018. YAP/TAZ upstream signals and downstream responses. Nat. Cell Biol. 20, 888–899.
Vance, R.J., Miller, D.C., Thapa, A., Haberstroh, K.M., Webster, T.J., 2004. Decreased fibroblast cell density on chemically degraded poly-lactic-co-glycolic acid, polyurethane, and polycaprolactone. Biomaterials 25, 2095–2103.
Wrighton, K.H., 2011. Mechanotransduction: YAP and TAZ feel the force. Nat. Rev. Mol. Cell Biol. 12, 404.
Yixiang, D., Yong, T., Liao, S., Chan, C.K., Ramakrishna, S., 2008. Degradation of electrospun nanofiber scaffold by short wave length ultraviolet radiation treatment and its potential applications in tissue engineering. Tissue Eng. Part A 14, 1321–1329.
Yu, D., Neeley, W.L., Pritchard, C.D., Slotkin, J.R., Woodard, E.J., Langer, R., Teng, Y.D., 2009. Blockade of peroxynitrite-induced neural stem cell death in the acutely injured spinal cord by drug-releasing polymer. Stem Cells 27, 1212–1222.
Yu, D., Thakor, D.K., Han, I., Ropper, A.E., Haragopal, H., Sidman, R.L., Zafonte, R., Schachter, S.C., Teng, Y.D., 2013. Alleviation of chronic pain following rat spinal cord compression injury with multimodal actions of huperzine a. Proc. Natl. Acad. Sci. U. S. A. 110, E746–E755.
Zhubanchaliyev, A., Temirbekuly, A., Kongrtay, K., Wanshura, L.C., Kunz, J., 2016. Targeting mechanotransduction at the transcriptional level: YAP and BRD4 are novel therapeutic targets for the reversal of liver fibrosis. Front. Pharmacol. 7, 462.